Advances in Aircraft and Spacecraft Science, *Vol. 1, No. 2 (2014) 177-196*
DOI: http://dx.doi.org/10.12989/aas.2014.1.2.177

Linking bilinear traction law parameters to cohesive zone length for laminated composites and bonded joints

Gang Li* and Chun Li

Aerospace, National Research Council Canada M-3, 1200 Montreal Road, Ottawa, Ontario, Canada K1A 0R6

(Received July 18, 2013, Revised October 5, 2013, Accepted November 1, 2013)

Abstract. A theoretical exploration for determining the characteristic length of the cohesive zone for a double cantilever beam (DCB) specimen under mode I loading was conducted. Two traction-separation laws were studied: (i) a law with only a linear elastic stage from zero to full traction strength; and (ii) a bilinear traction law illustrating a progressive softening stage. Two analytical solutions were derived for the first law, which fit well into two existing solution groups. A transcendental equation was derived for the bilinear traction law, and a graphical method was presented to identify the resultant cohesive zone length. The study using the bilinear traction law enabled the theoretical investigation of the individual effects of cohesive law parameters (i.e., strength, stiffness, and fracture energy) on the cohesive zone length. Correlations between the theoretical and finite element (FE) results were assessed. Effects of traction law parameters on the cohesive zone length were discussed.

Keywords: cohesive zone length; traction law; theoretical solutions

1. Introduction

Adhesive bonding, in lightweight sandwich construction and structural bonded joints, has been used for decades for the assembly of aircraft components. There has been a recent increase in the application of adhesive bonding in modern aircraft, largely driven by the usage of advanced carbon fibre composite materials. However, in-service experience has shown that the durability of bonded structures and adhesively bonded repairs varies dramatically, with some structures and repairs providing life-of-type service and others failing in a very short time, leading to a reluctant acceptance by aircraft operators as pointed by Davis and Bond (1999). In addition, due to difficulty in detecting the damage evolution of the adhesive bond and delamination, catastrophic failure could occur in the laminated structures (Ashtonm 1996, Li *et al*. 2012, Li 2013).

Delamination and disbond belong to the most important damage mechanisms in laminates and bonded laminated joint structures. To understand the performance of composite structures and associated delamination onset and propagation, standard tests combined with finite element (FE) simulations have been widely conducted. Numerical methodologies using FE methods integrated with techniques such as the virtual crack closure technique (VCCT) and/or cohesive zone models (CZMs) using cohesive elements or surfaces have been developed to capture the crack onset and to simulate progressive failure (Rybicki and Kanninen 1977, Krueger 2004, Mi *et al*. 1998, Alfano

*Corresponding author, Ph.D., E-mail: Gang.Li@nrc-cnrc.gc.ca

http://www.techno-press.org/?journal=aas&subpage=7 ISSN: 2287-528X (Print), 2287-5271 (Online)

2006). VCCT originates from a fracture mechanics concept, in which the strain energy released during delamination propagation is assumed to equal the work required to close the crack. Crack growth will occur if the energy release rate reaches a critical value. This scheme needs nodal forces and topological information from nodes ahead and behind the crack tip. CZM has been developed from the work of Barrenblatt and Dugdale by assuming a cohesive zone existed just ahead of a physical crack tip. The stress traction within the zone is used to model cohesive tractions or plastic yielding, which makes that the CZM be a powerful approach for the progressive failure analysis of composite structures under various loading conditions (Mi *et al.* 1998, Alfano 2006, Turon *et al.* 2007a, b, de Moura *et al.* 2008, Harper and Hallett 2008, Khoramishad *et al.* 2010, Landry and Laplante 2012).

A local cohesive traction-separation (i.e., stress-displacement) relationship is used to govern the behaviour of the nodal pairs of the cohesive elements to capture the damage propagation. The shape of the traction-separation curves can be different; however, the total area enclosed by any curve shape must equal the critical strain energy release rate of the material under a quasi-static loading (Turon *et al.* 2007b, Harper and Hallett 2008). Previously, difficulty was existed to experimentally determine the traction profile; it was usually deduced indirectly based on physical material behaviour. Nowadays, direct methods based on experimental determination of the cohesive traction profile using the DCB test can be used (Andersson and Biel 2006, Ji *et al.* 2010, Dias, *et al.* 2013). The strain energy release rate G_I or J-integral should be expressed in a function of the crack tip opening displacement or applied load and beam rotation in these methods, then the cohesive traction law can be obtained by differentiation of the G_I or J-integral. Williams and Hadavinia (2002) carried out analytical solutions for several different cohesive zone traction laws for the case of a beam on an elastic foundation. They showed that all the solutions gave very similar results for the energy release rate and beam root rotation; only the fracture toughness was a critical parameter in the delamination analysis. Yang and Cox (2005) used a bridging length solution proposed by Bao and Sou (1992) to estimate the characteristic length of the cohesive zone. The theoretical solutions showed that different cohesive zone lengths were generated by different traction laws. These analytical solutions for the cohesive zone length provide a basis to assess a proper cohesive element length mesh for a converged FE simulation of progressive failure behaviour. To the end, it was suggested by Turon *et al.* (2007b) and Harper and Hallett (2008) that at least three cohesive elements should be placed within a fully developed cohesive zone length in the FE analysis.

Currently, none of existing analytical solutions for the cohesive zone length have been derived from a mode I double cantilever beam (DCB) configuration using a bilinear cohesive traction-separation law. For delamination study, a mode I loading DCB configuration would be adopted first due to its high applicability and importance. A bilinear cohesive traction-separation law is widely used in numerical simulations due to its simplicity and versatility. This law is characterized by an elastic region up to full strength followed by a softening region until a complete nodal pair separation at zero traction. The cohesive zone length used for choosing cohesive element length was estimated based on the available analytical solutions.

In this paper, theoretical explorations were carried out to determine the cohesive zone lengths for mode I loading DCB specimens. Two traction laws were selected: (i) a right-angled triangular form having only a linear elastic stage from zero to full strength followed by a sudden catastrophic failure; and (ii) a bilinear traction law. Theoretical determinations of the cohesive zone length were developed. Comparison of current, existing theoretical predictions, and FE results was conducted and discussed. Effects of cohesive traction law parameters on the cohesive zone length could be

theoretically assessed. The main objective was to develop analytical solutions of cohesive zone length in DCB configuration with the bilinear traction law, and expand the theoretical knowledge on the correlation between traction law parameters for accurate numerical progressive failure simulations.

2. Theoretical derivation

2.1 Two typical cohesive traction-separation laws

A variety of cohesive traction-separation laws have been used for theoretical fracture behaviour analysis, among which two laws in the simplest forms have been chosen for a comparative study in this paper, as shown in Fig. 1, where σ_0 is the interfacial strength; *K*: the interfacial stiffness ($K = \sigma_0 / \delta_0$); δ_0: displacement ($\delta_0 = 2w_0$ for the DCB case, where w_0 is the half relative displacement at a given integration point in the vicinity of crack tip determined by the beam deflection at this moment) at the irreversible interface damage initiation position, and δ_f: the relative displacement for separation ($\delta_f = 2w_f$ for the DCB case, where w_f is the beam deflection), where the traction is degraded to zero. For the DCB case, the critical strain energy release rate is computed as: $G_c = 1/2\sigma_0\delta_f = \sigma_0 w_f$. Fig. 1(a) shows an idealized traction law in a right-angled triangular form. Fig. 1(b) shows a bilinear traction law with a progressive linear damage stage (or softening stage not perpendicular to the horizontal axis) after the damage onset at $\sigma = \sigma_0$. This bilinear traction profile effectively reduces the numerical singularity degree. The right-angled traction law actually cannot provide converged solutions in numerical analyses due to its abrupt stress cancellation. However, this law selected here for the study based on two reasons: (1) to effectively illustrate the advantages of the bilinear traction law in progressive damage analysis, and (2) to explore analytical solution of its cohesive zone length for correlation study with other existing solutions.

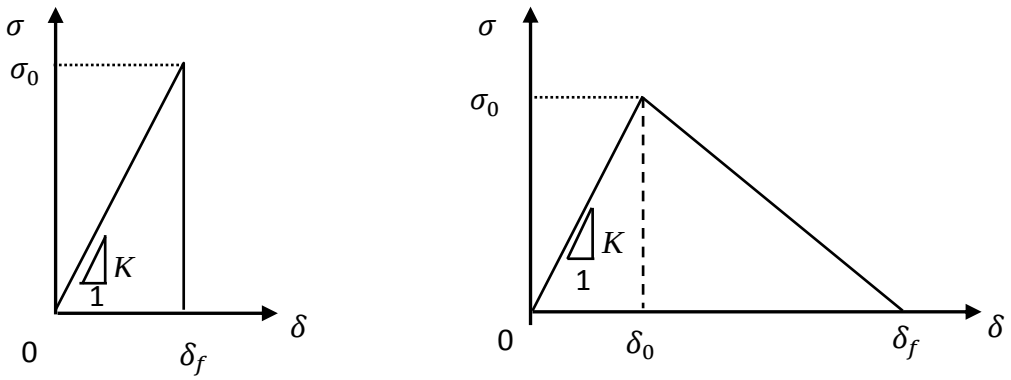

Fig. 1 Two cohesive traction-separation laws: (a) a linear elastic stage followed by a sudden catastrophic separation in a right-angled triangular form, and (b) a bilinear relationship

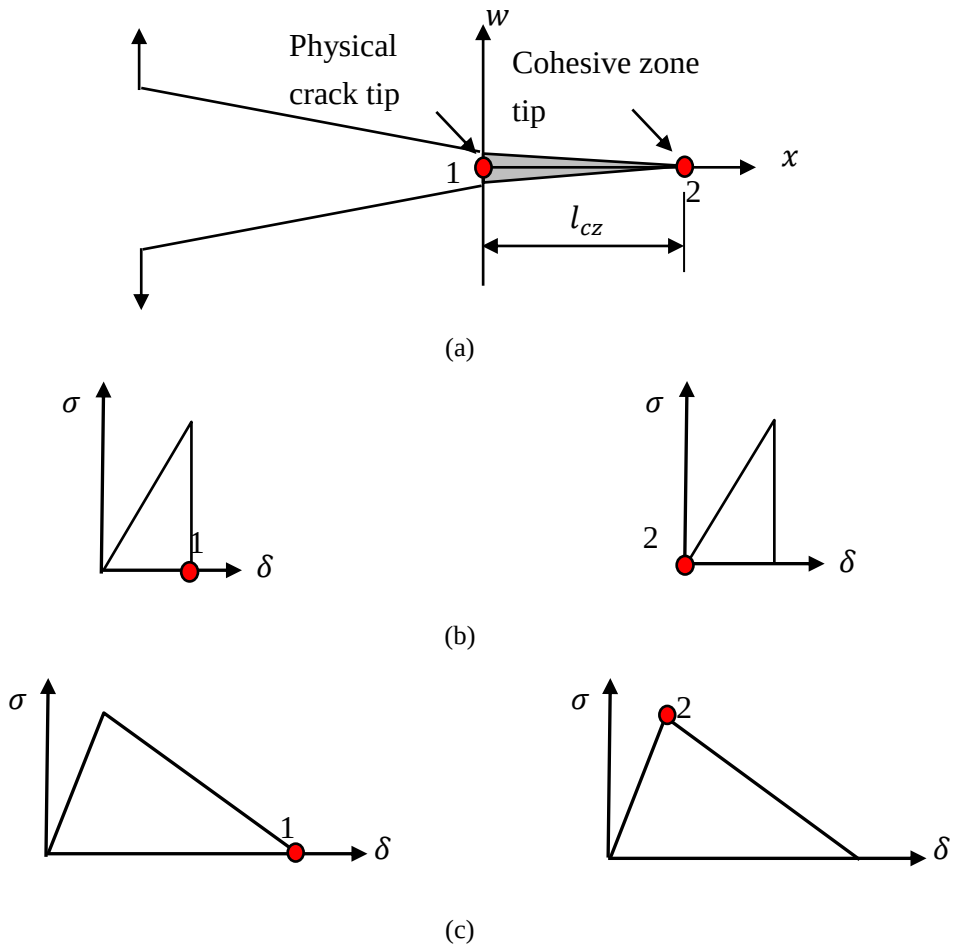

Fig. 2 Schematic diagrams for: (a) the characteristic length of a fully developed cohesive zone, l_{cz}, located ahead of the physical crack tip; and determination of the l_{cz} in: (b) a right-angled triangular traction law form, and (c) a bilinear traction law

A cohesive zone with zero- or very small thickness can be introduced into a structure for capturing the progressive failure behaviour. The characteristic length of a fully developed cohesive zone length, l_{cz}, can be determined using the conditions shown in Fig. 2. Labels "1" and "2" refer to the physical crack and cohesive zone tips, as well as their traction/separation conditions for defining the fully developed cohesive zone length. At the physical crack tip, the laminated beam deflection is defined as $w(0) = 0.5\delta_f$ at position 1. For the right-angled triangular traction form Eq. (1(a)) may be used to identify the value of l_{cz} at position 2.

$$w(x)\big|_{x=l_{cz}} = 0 \tag{1a}$$

For the bilinear traction law at position 2, the following condition, Eq. (1(b)), is widely used to identify the value of l_{cz}.

$$w(x)\big|_{x=l_{cz}} = 0.5\delta_0 \tag{1b}$$

2.2 Cohesive zone length for the right-angled triangular traction law

2.2.1 Beam deflection and associated energy release rate

The augmented double cantilever beam (DCB) model proposed by Kanninen (1973) was adopted, and the DCB arm was theoretically treated as a beam partially supported by an elastic foundation, as shown in Fig. 3.

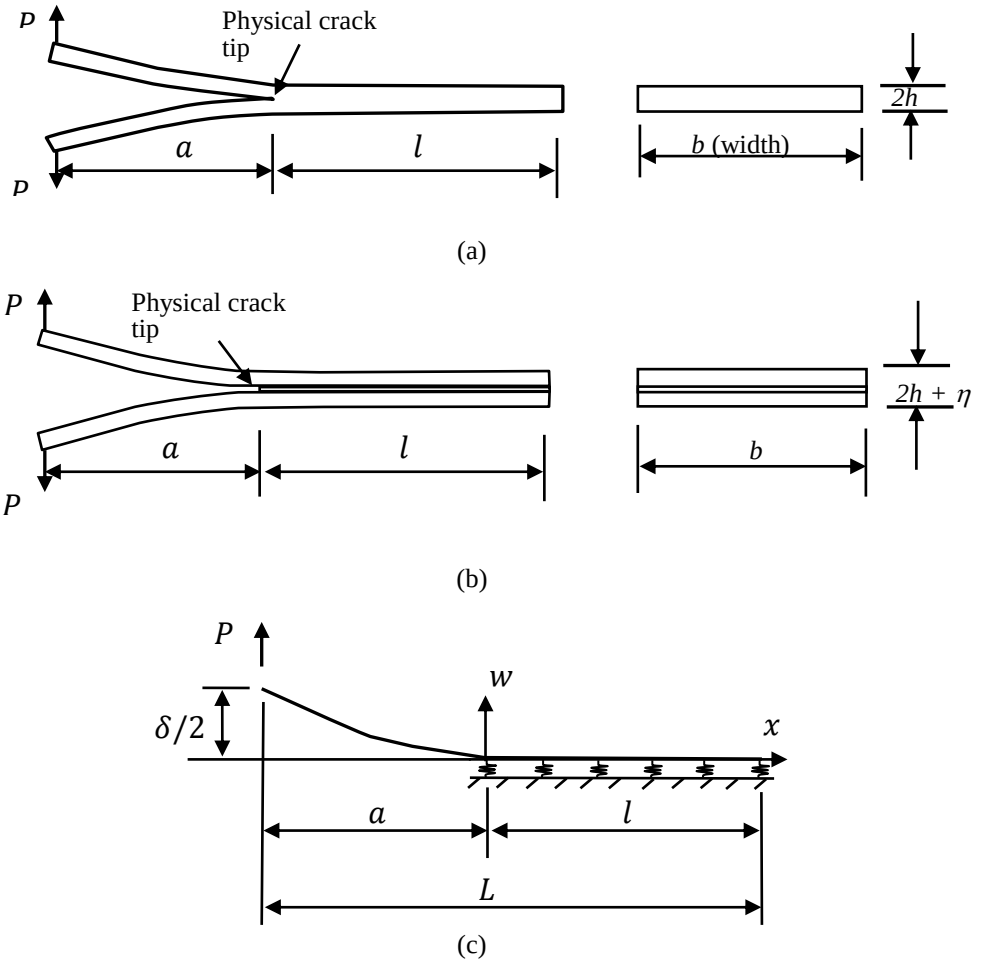

Fig. 3 Schematic representation of: (a) a DCB coupon made of a single-piece of material, (b) a bonded DCB coupon, and (c) the augmented double cantilever beam model for mode I fracture (not to scale)

The symbols used are: a: the delamination length; b: the DCB width; h: the laminate thickness; l: un-delaminated or bonded length; L: the total length of the DCB coupon; δ: the DCB opening displacement at the applied load position; and η: the adhesive thickness. The Euler-Bernoulli beam theory has been widely used to analyze the DCB beam deflection (Kanninen 1973, Chow *et al.* 1979, Krenk 1992, Williams and Hadavinia 2002, Li *et al.* 2011, Li and Li 2013). The corresponding governing differential equations for the laminated DCB beam deflection $w(x)$ are

$$\begin{aligned} D\frac{d^2w_1}{dx^2} &= P(a+x) \qquad (-a < x \le 0) \\ D\frac{d^4w_2}{dx^4} &= -kw \qquad (0 \le x \le l) \end{aligned} \tag{2a}$$

where; w_1 is the deflection within the delaminated range; w_2: deflection within the bonded overlap region; D: the bending stiffness of cylindrical bent laminates (plane strain condition); k: the spring stiffness simplified for the adhesive layer in bonded DCB coupons or the influence of the opposite side beam; and P: the applied load. Determination of the parameter D is given by Li *et al.* (2011).

The relationship between the spring stiffness, k, fracture energy, G_c, interfacial strength, σ_0, and relative displacement, w_0, (here w_0=w_f)may be explained as

$$k = \frac{b\sigma_0}{w_f} = \frac{b\sigma_0}{G_c/\sigma_0} = \frac{b\sigma_0^2}{G_c} \tag{2b}$$

The general solution of the beam deflection is

$$\begin{aligned} w_1(x) &= \frac{P}{D}\left(\frac{1}{6}(a+x)^3 + A_0(a+x) + A_1\right) \qquad (-a < x \le 0) \\ w_2(x) &= A_2\cosh(\lambda x)\cos(\lambda x) + A_3\sinh(\lambda x)\cos(\lambda x) \\ &\quad + A_4\cosh(\lambda x)\sin(\lambda x) + A_5\sinh(\lambda x)\sin(\lambda x) \qquad (0 \le x \le l) \end{aligned} \tag{2c}$$

where $\lambda^4 = k/(4D)$ is a parameter defined in the bending analysis. Using the following six displacement boundary conditions

$$\begin{aligned} &w_1(0) = w_2(0), \quad \left.\frac{dw_1(x)}{dx}\right|_{x=0} = \left.\frac{dw_2(x)}{dx}\right|_{x=0}, \quad \left.\frac{d^2w_1(x)}{dx^2}\right|_{x=0} = \left.\frac{d^2w_2(x)}{dx^2}\right|_{x=0} \\ &\left.\frac{d^3w_1(x)}{dx^3}\right|_{x=0} = \left.\frac{d^3w_2(x)}{dx^3}\right|_{x=0}, \quad \left.\frac{d^2w_2(x)}{dx^2}\right|_{x=l} = 0, \text{ and } \left.\frac{d^3w_2(x)}{dx^3}\right|_{x=l} = 0 \end{aligned} \tag{2d}$$

the six integral constants A_i (i=0 to 5) can be determined as

$$A_0 = -\frac{H_1}{2\lambda^2} - \frac{a^2}{2}, \quad A_1 = \frac{H_2}{2\lambda^3} + \frac{aH_1}{2\lambda^2} + \frac{a^3}{3}, \quad A_2 = \frac{P}{2D\lambda^3} H_2$$
$$A_3 = -\frac{P}{2D\lambda^3}\left(\frac{H_1+1}{2}\right), \quad A_4 = -\frac{P}{2D\lambda^3}\left(\frac{H_1-1}{2}\right), \text{ and } \quad A_5 = \frac{Pa}{2D\lambda^2} \tag{2e}$$

where H_1, H_2, $a\lambda$, and λl are dimensionless factors as

$$H_1 = \frac{\sinh^2(\lambda l) + \sin^2(\lambda l)}{\sinh^2(\lambda l) - \sin^2(\lambda l)} + 2a\lambda \frac{\sinh(\lambda l)\cosh(\lambda l) + \sin(\lambda l)\cos(\lambda l)}{\sinh^2(\lambda l) - \sin^2(\lambda l)}$$
$$H_2 = \frac{\sinh(\lambda l)\cosh(\lambda l) - \sin(\lambda l)\cos(\lambda l)}{\sinh^2(\lambda l) - \sin^2(\lambda l)} + a\lambda \frac{\sinh^2(\lambda l) + \sin^2(\lambda l)}{\sinh^2(\lambda l) - \sin^2(\lambda l)} \tag{2f}$$

when $\lambda l \geq 3$, $\sinh(\lambda l) \approx \cosh(\lambda l)$ and they are significantly greater than $\sin(\lambda l)$ and $\cos(\lambda l)$. Then similar to Williams and Hadavinia (2002), the defection, w_2, becomes

$$w_2(x) = \exp(-\lambda x)(A_2 \cos(\lambda x) + A_4 \sin(\lambda x)) \qquad (0 \leq x \leq l)$$
$$H_1 = 1 + 2a\lambda, \quad H_2 = 1 + a\lambda \tag{2g}$$

For a fully developed cohesive zone, the deflection condition at the physical crack tip is: $w_1(0) = w_2(0) = w_f$ and thus, $A_2 = PH_2/(2D\lambda^3) = w_f$. The critical strain energy release rate, G_c, is obtained as

$$G_c = \frac{P_c^2}{bD\lambda^2}\left(H_1 + a^2\lambda^2\right) = \frac{(P_c a)^2}{bD}\left(1 + \frac{1}{a\lambda}\right)^2\Bigg|_{\text{when } \lambda l \geq 3} \tag{2h}$$

It can be seen that λ is an important parameter to determine the deflection and strain energy release rate.

2.2.2 Cohesive zone length

2.2.2.1 Solution one

Using the approach of Williams and Hadavinia (2002), the characteristic length of a cohesive zone, l_{cz}, can be defined based on the deformation process parameter, λ, as

$$\frac{1}{\lambda^4} = \frac{4D}{k} = \frac{4DG_c}{b\sigma_0^2} = h^3\left(\frac{E'G_c}{3\sigma_0^2}\right) = h^3 l_{cz}, \text{ and } \quad l_{cz} = \frac{E'G_c}{3\sigma_0^2} \tag{3a}$$

where

$E' = E$ (plane stress) or $E' = E/(1-\nu^2)$ (plane strain) for isotropic material DCB,
and $E' = D/I_z$ (equivalent flexural modulus for laminated DCB) (3b)

I_z is the moment of inertia in the bending analysis. The laminate bending stiffness, D, under

either plane stress or plane strain (cylindrical bending) is given by Li *et al.* (2011). The current solution, Eq. (3(a)), is half of the one derived by Williams and Hadavinia (2002) for a single peeling beam from a stiff foundation. The relationship $G_c = 0.5\sigma_0 w_f$ was used in l_{cz} derivation by them. Hence, the solution presented in their paper will be updated to the current solution for DCB specimens.

2.2.2.2 Solution two

An alternative way to determine l_{cz} is based on the beam deflection condition, as presented in Eq. (1(a)) combined with Fig. 2, $w(x)\big|_{x=l_{cz}}$ (i.e., $\sigma(x)\big|_{x=l_{cz}}$ at position 2). The first or smallest x value will be the l_{cz}, since other values have no practical value and also cause numerical solution problems. For most DCB cases, $\lambda l \geq 3$ can be established, and the associated l_{cz} is

$$l_{cz} = \frac{1}{\lambda}\arctan\left(\frac{1+a\lambda}{a\lambda}\right) \tag{3c}$$

When $a\lambda$ is very large, the above expression can be simplified as

$$\lim_{a\lambda\to\infty} l_{cz} = \frac{\pi}{4\lambda} = 0.6\left(\frac{E'G_c}{\sigma_0^2}\right)^{\frac{1}{4}} h^{\frac{3}{4}} \tag{3d}$$

Different l_{cz} values would be predicted by Eqs. (3(a)) and (3(c)). Eq. (3(c)) is equivalent to Eq. (3(d)) for large values of $a\lambda$. Comparisons of the predicted characteristic length profiles with existing solutions are conducted later in the paper.

2.3 Cohesive zone length for the bilinear traction law

2.3.1 Beam deflection and associated energy release rate

Fig. 4 shows two parallel coordinate frames used for the beam deflection analysis within the two different traction-separation stages. The distance between the two origins is the length for a fully developed cohesive zone, l_{cz}, and l_R refers to the undamaged laminate or bondline length.

The corresponding deflection equations in each section are

$$\begin{aligned}
&\frac{d^2w}{dx^2} = \frac{P}{D}(a+x) && (-a < x_1 \leq 0)\\
&\frac{d^4(w_1 - w_f)}{dx^4} = 4\lambda_1^4(w_1 - w_f) && (0 \leq x_1 \leq l_{CZ})\\
&\frac{d^4w_2}{dx^4} = -4\lambda_2^4 w_2 && (x_2 > 0)
\end{aligned} \tag{4a}$$

where $\lambda_1^4 = \frac{b\sigma_0}{4D(w_f - w_0)}$ and $\lambda_2^4 = \frac{k}{4D} = \frac{b\sigma_0}{4Dw_0}$.

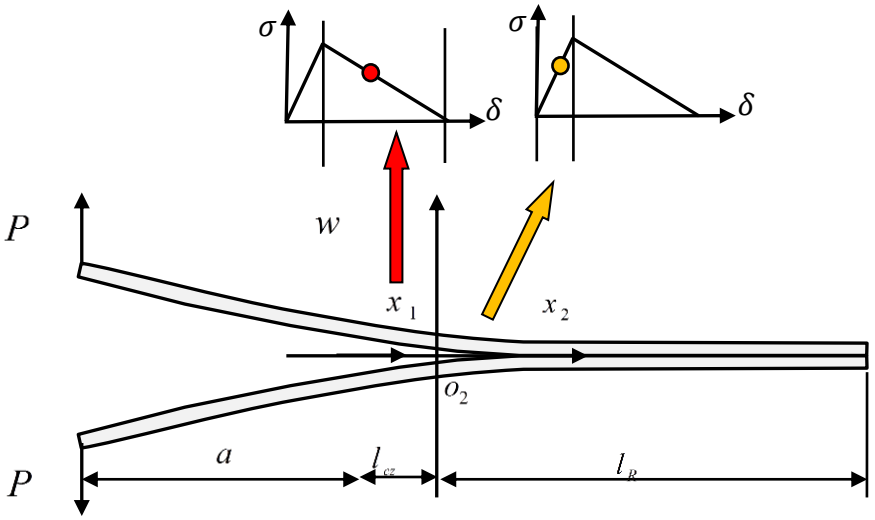

Fig. 4 Schematic diagrams for coordinates at the physical crack and cohesive zone tips (o_1 and o_2, respectively) and correlation of the beam deflection with its associated cohesive traction-separation stage, where l_{cz} and l_R refer to the fully developed cohesive zone length and the undamaged laminate length, respectively (not to scale)

For simplicity, the undamaged laminate length is assumed to be long enough, $\lambda_2 l_R \geq 3$, so that general solutions become

$$w(x) = \frac{P}{D}\left(\frac{1}{6}(a+x)^3 + B_0(a+x) + B_1\right)$$

$$w_1(x) = w_f + B_2\cosh\sqrt{2}\lambda_1 x + B_3\sinh\sqrt{2}\lambda_1 x + B_4\cos\sqrt{2}\lambda_1 x + B_5\sin\sqrt{2}\lambda_1 x \tag{4b}$$

$$w_2(x) = e^{-\lambda_2 x}\left(B_6\cos\lambda_2 x + B_7\sin\lambda_2 x\right)$$

A total of nine boundary conditions are used to determine the eight above constants B_i (i = 0 to 7) and l_{cz}. They are

$$w(0) = w_1(0) = w_f, \qquad \left.\frac{dw(x)}{dx}\right|_{x=0} = \left.\frac{dw_1(x)}{dx}\right|_{x=0}$$

$$\left.\frac{d^2w(x)}{dx^2}\right|_{x=0} = \left.\frac{d^2w_1(x)}{dx^2}\right|_{x=0}, \qquad \left.\frac{d^3w(x)}{dx^3}\right|_{x=0} = \left.\frac{d^3w_1(x)}{dx^3}\right|_{x=0} \tag{4c}$$

$$w_1(l_{cz}) = w_2(0) = w_c, \qquad \left.\frac{dw_1(x)}{dx}\right|_{x=l_{cz}} = \left.\frac{dw_2(x)}{dx}\right|_{x=0}$$

$$\left.\frac{d^2w_1(x)}{dx^2}\right|_{x=l_{cz}} = \left.\frac{d^2w_2(x)}{dx^2}\right|_{x=0}, \qquad \left.\frac{d^3w_1(x)}{dx^3}\right|_{x=l_{cz}} = \left.\frac{d^3w_2(x)}{dx^3}\right|_{x=0}$$

$$\text{and} \quad \left.\frac{d^4w_1(x)}{dx^4}\right|_{x=l_{cz}} = \left.\frac{d^4w_2(x)}{dx^4}\right|_{x=0}.$$

The obtained constants are

$$B_0 = \frac{D}{P}\sqrt{2}\lambda_1(B_3 + B_5) - \frac{1}{2}a^2, \qquad B_1 = \frac{D}{P}w_f - \frac{1}{6}a^3 - B_0 a$$

$$B_2 = -B_4 = \frac{1}{4\lambda_1^2}\frac{Pa}{D}, \qquad B_2 = \frac{I_1 I_{12} - I_0 I_{22}}{I_{11}I_{22} - I_{12}I_{21}}, \qquad B_3 = -\frac{1}{I_{12}}(I_0 + B_2 I_{11})$$

$$B_5 = B_3 - \frac{1}{2\sqrt{2}\lambda_1^3}\frac{P}{D}, \quad B_6 = -\frac{\lambda_1^4}{\lambda_2^4}\left(B_2(C-c) + B_3(S+s) - \frac{s}{2\sqrt{2}\lambda_1^3}\frac{P}{D}\right) \tag{4d}$$

$$B_7 = -\frac{\lambda_1^2}{\lambda_2^2}\left(B_2(C+c) + B_3(S-s) + \frac{s}{2\sqrt{2}\lambda_1^3}\frac{P}{D}\right), \quad w_0 = B_6, \quad w_f = \left(1 + \frac{\lambda_2^4}{\lambda_1^4}\right)w_0$$

where

$$C = \cosh\sqrt{2}\lambda_1 l_{cz}, \quad c = \cos\sqrt{2}\lambda_1 l_{cz}, \quad S = \sinh\sqrt{2}\lambda_1 l_{cz}, \text{ and } \quad s = \sin\sqrt{2}\lambda_1 l_{cz}$$

$$I_0 = \frac{\sqrt{2}}{4\lambda_1^3}\frac{P}{D}\left(-\frac{\sqrt{2}}{2}\left(1 - \frac{\lambda_1^2}{\lambda_2^2}\right)c + \frac{\lambda_1}{\lambda_2}s\right), \quad I_0^a = \left(-\frac{\sqrt{2}}{2}\left(1 - \frac{\lambda_1^2}{\lambda_2^2}\right)c + \frac{\lambda_1}{\lambda_2}s\right)$$

$$I_1 = \frac{\sqrt{2}}{4\lambda_1^3}\frac{P}{D}\left(\frac{\sqrt{2}}{2}\left(1 + \frac{\lambda_1^2}{\lambda_2^2}\right)c - \frac{\lambda_1^3}{\lambda_2^3}s\right), \quad I_1^a = \left(\frac{\sqrt{2}}{2}\left(1 + \frac{\lambda_1^2}{\lambda_2^2}\right)c - \frac{\lambda_1^3}{\lambda_2^3}s\right) \tag{4e}$$

$$I_{11} = \frac{\sqrt{2}}{2}(S+s) + \frac{\sqrt{2}}{2}\frac{\lambda_1^2}{\lambda_2^2}(S-s) + \frac{\lambda_1}{\lambda_2}(C+c), \quad I_{12} = \frac{\sqrt{2}}{2}(C+c) + \frac{\sqrt{2}}{2}\frac{\lambda_1^2}{\lambda_2^2}(C-c) + \frac{\lambda_1}{\lambda_2}(S-s)$$

$$I_{21} = -\frac{\sqrt{2}}{2}(S+s) + \frac{\sqrt{2}}{2}\frac{\lambda_1^2}{\lambda_2^2}(S-s) + \frac{\lambda_1^3}{\lambda_2^3}(C-c), \text{ and } \quad I_{22} = -\frac{\sqrt{2}}{2}(C+c) + \frac{\sqrt{2}}{2}\frac{\lambda_1^2}{\lambda_2^2}(C-c) + \frac{\lambda_1^3}{\lambda_2^3}(S+s)$$

The critical strain energy release rate, G_c, can be expressed as

$$G_c = \frac{1}{2}\sigma_0\delta_f = 2Kw_0w_f = 2K\left(1+\frac{\lambda_2^4}{\lambda_1^4}\right)w_0^2 \tag{4f}$$

where

$$w_0 = B_6 = -\frac{\lambda_1^4}{\lambda_2^4}B_2\left[(C-c)-\frac{I_{11}}{I_{12}}(S+s)-\frac{\sqrt{2}}{a\lambda_1}\frac{(S+s)\left(-c+\frac{\lambda_1^2}{\lambda_2^2}c+\sqrt{2}\frac{\lambda_1}{\lambda_2}s\right)}{C+c+\frac{\lambda_1^2}{\lambda_2^2}(C-c)+\sqrt{2}\frac{\lambda_1}{\lambda_2}(S-s)}-\frac{\sqrt{2}}{a\lambda_1}s\right] \tag{4g}$$

2.3.2 Determination of the cohesive zone length

Based on the above boundary conditions, the cohesive zone length, l_{cz}, can be determined using the derived relationship as

$$B_2 = \frac{I_1I_{12}-I_0I_{22}}{I_{11}I_{22}-I_{12}I_{21}} = \frac{1}{4\lambda_1^2}\frac{Pa}{D} \tag{5a}$$

or

$$\frac{I_{11}I_{22}-I_{12}I_{21}}{I_1^aI_{12}-I_0^aI_{22}} = \frac{\sqrt{2}}{a\lambda_1} \tag{5b}$$

An analytical expression for l_{cz} is not easily derived. Therefore, a graphical method is suggested to identify the root (i.e., the characteristic length) from the following transcendental Eq. (5(c)) obtained from Eq. (5(a)) or (5(b)). Provided that all relevant parameters are known, changes to variable x can be made starting from a very small value using a reasonably fine increment; the minimum x that makes the following two y-functions meet is the characteristic length, l_{cz}. If $a\lambda_1$ is very large, *y1=0* can be approximated.

$$\begin{cases} y_1 = \dfrac{\sqrt{2}}{a\lambda_1} \\ y_2 = \dfrac{I_{11}I_{22}-I_{12}I_{21}}{I_1^aI_{12}-I_0^aI_{22}} \end{cases} \tag{5c}$$

2.4 Existing analytical solutions for the cohesive zone length

The characteristic length expressions for an infinite body made of an isotropic material with a central crack loaded in mode I have been derived by a number of authors using different cohesive traction laws, as listed in the paper of Turon *et al.* (2007b). It can be represented as

$$l_{cz} = \gamma\frac{E'G_c}{\sigma_0^2} \tag{6a}$$

where $E' = E$ (plane stress) or $E' = E/(1-\nu^2)$ (plane strain), and γ is a coefficient derived from the specific used cohesive traction law. An asymptotic expression with $\gamma = 1$ for estimating

the characteristic length suggested by Yang and Cox (2005) for orthotropic materials is

$$l_{cz} = \frac{E'G_c}{\sigma_0^2} \tag{6b}$$

where E' is an equivalent elastic modulus for orthotropic materials. Determination of the modulus is presented in papers of Harper and Hallett (2008), and Yang *et al.* (2006).

For delamination in a slender laminated body similar to an infinite mode I loading DCB specimen, Yang and Cox (2005) set a unity coefficient to the bridging length derived by Bao and Sou (1992) to estimate the cohesive zone length, as follows

$$l_{cz-slender} = \left(\frac{E'G_c}{\sigma_0^2}\right)^{\frac{1}{4}} h^{\frac{3}{4}} \tag{6c}$$

In the derivation of characteristic length, Bao and Sou (1992) applied a constant moment to the slender beam ends. The utilized cohesive traction law has non-zero traction at the zero separation condition. It can be noticed that Eqs. (6(a)) and (6(c)) are different and may be divided into two solution groups based on their expressions.

2.5 Stiffness K in the cohesive traction-separation law

2.5.1 A fixed value determined by the laminated DCB parameters

The elastic foundation assumption, proposed by Kanninen (1973), could be used to define the associated traction-separation law of the introduced cohesive zone. Hence, a fixed interfacial stiffness, K, of the cohesive traction law is obtained from the DCB parameters

$$k = 2Kb = \frac{2E_z^{'}b}{h} \qquad \text{(for monolithic DCB coupon)} \tag{7a}$$

$$k = 2Kb = \frac{2E_a^{'}b}{\eta} \qquad \text{(for bonded DCB coupon)} \tag{7b}$$

where k is the spring stiffness introduced by the assumed elastic foundation; b: the DCB coupon width; h: the DCB beam thickness in one side; E_z': the laminated beam Young's modulus in the peeling direction under plane strain conditions; E_a': the adhesive Young's modulus under plane strain conditions; and η: adhesive layer thickness for the bonded DCB coupon.

2.5.2 A variable without a direct linkage to the laminated coupon parameters

The experimentally obtained critical energy release rate is used in the cohesive law. The stiffness K and strength σ_0 have no direct relationship with the tested DCB coupons. Thus, different values of K and σ_0 can be selected for the numerical progressive failure analysis. As pointed by Zou *et al.* (2003), the stiffness should be large enough to exclude the effect of the introduced cohesive zone on the original material property but small enough to avoid numerical problem in a finite element analysis. Through modeling analysis of damage in filament-wound pipes, they found that its effect on the load-indentation was limited when the K was in the range

$$K = f\sigma_0 \qquad (f = 10^4 - 10^7 \ \text{mm}^{-1}) \tag{7c}$$

2.5.3 Correlation of K with cohesive law parameters

For the right-angled triangular traction law, the correlation between K, G_c and σ_0 is

$$K = \frac{\sigma_0^2}{2G_c} \tag{7d}$$

This relationship shows that no two parameters can be kept constant simultaneously, if the third one changes.

For the regular bilinear traction law, the condition, $w_0 < w_f$, should be kept to ensure a progressive linear softening stage. Therefore, the selected stiffness must satisfy the condition

$$K > \frac{\sigma_0^2}{2G_c} \tag{7e}$$

A remarkable advantage of this law over the right-angled triangular traction law is that any two parameters among K, G_c, and σ_0 can be kept as invariable simultaneously when the third one changes. This allows us to study the individual effects of K, G_c, or σ_0 on l_{cz}.

Based on relationships, $\delta_0 = \sigma_0 / K$ and $\delta_f = 2G_c/\sigma_0$, the following correlations can be established

$$\lambda_1 = \lambda_2 \left(\frac{1}{2G_c K/\sigma_0^2 - 1} \right)^{\frac{1}{4}}, \quad \lambda_2 = \left(\frac{bK}{2D} \right)^{\frac{1}{4}} \tag{7f}$$

Hence, the effects of K, G_c, and σ_0 on l_{cz} can be numerically studied using Eq. (5(c)) by the aid of Eq.(7(f)) for any specific DCB coupon.

3. Results and discussion

3.1 Correlation of the cohesive zone length with the existing solutions

Regardless of different geometric conditions and traction-separation laws used, it can be seen that the current solution in Eq. (3(a)) belongs to the group of Eq. (6(a)) with a coefficient of $\gamma = 1/3$. This solution is almost identical to Irwin's solution presented in the paper of Turon *et al.* (2007b). The solution, Eq. (3(d)), is approximately 0.6Eq. (6(c)), in the other group. For the bilinear cohesive traction-separation law, a graphical method is suggested to be used to predict the characteristic length. Comparison of the characteristic lengths obtained from relevant theoretical analyses can be conducted to assess the existing correlation.

Table 1 Parameters used in FE simulation of unidirectional 0 °laminated DCB coupons (refer to Fig. 3)

3.2 Comparison of cohesive zone lengths

Table 1 Parameters used in FE simulation of unidirectional 0 °laminated DCB coupons (refer to Fig. 3)

Example 1: HTA6376/C laminated DCB coupon
Geometry: L = 150 mm; a = 35 mm; b = 20 mm; h = 1.55 mm.
Laminate properties: G_c = 0.26 N/mm; σ_0 = 30 MPa; K = 1x10^5 N/mm^3; E_{11} = 120 GPa; E_{22} = 10.5 GPa; G_{12} = 5.25 GPa; G_{23} =3.48 GPa; $v_{12} = v_{13}$ = 0.3; v_{23} = 0.51.
Example 2 : T300/977-2 laminated DCB coupon
Geometry: L = 150 mm; a = 55 mm; b = 20 mm; h = 1.98 mm.
Laminate properties: G_c = 0.325 N/mm; σ_0 = 60 MPa; K = 1x10^5 N/mm^3; E_{11} = 150 GPa; E_{22} = 11 GPa; G_{12} = 6 GPa; G_{23} =3.7 GPa; $v_{12} = v_{13}$ = 0.3; v_{23} = 0.51.

To have a clear comparison of this work with the open literature, examples from papers of Turon *et al.* (2007b) and Harper and Hallett (2008) were used. The material properties for unidirectional 0 °laminated DCB coupons are given in Table 1.

A constant element length of 0.125 mm was used in the FE analyses of Harper and Hallett (2008) to predict the fully developed cohesive zone lengths. The numerical cohesive zone lengths used in the current comparisons were obtained by visual judgment from their FE results. Small differences between the estimated FE values and the original data will exist; however, these will not affect the comparison. As pointed by Harper and Hallett (2008), a large difference was found between the analytical and FE results, a scaling factor of 0.5 was suggested to apply to Eqs. (6(b)) and (6(c)) for a good fit to the numerical results. The Eq. (6(c)) can be approximated to be Eq. (3(d)) in the comparison. Current solutions, Eqs. (3(a)) and (5(c)), were used for the comparison. This 0.5 factor was adopted here in Eq. (5(c)). No scaling factor was applied to Eq. (3(a)) since it has a small coefficient of 1/3. To be consistent with the work of Harper and Hallett (2008), the modulus E', in Eqs. (3(a)), (6(b)) and (6(c)), was determined using the method suggested by Yang and Cox (2005) and Yang *et al.* (2006). It should be noted that the bilinear traction-separation law was only used in the FE models and theoretical solution of Eq. (5(c)).

Figs. 5 and 6 show comparisons of the cohesive zone length obtained from theoretical and FE results for HTA6376/C and T300/977-2 DCB, respectively. Effects of several factors on the cohesive zone length were assessed. The results show that a large G_c or a small σ_0 will lead to a long cohesive zone length. To a lesser degree, an increase in E_{11}, E_{33}, G_{13} and h will extend l_{cz}. It can be seen that the current solution Eq. (3(a)) greatly reduced the difference with the FE results as per the used existing solution of Eq. (6(b)). Similarly, current solution of Eq. (3(d)), approximated by Eq. (6(c)), could have good agreement with FE results. The theoretical solutions, Eqs. (3(a)) and (6(b)), cannot show the effect of the beam thickness, h, while solutions from Eq. (5(c)) show little influence from E_{33} or G_{13} for the studied unidirectional 0 ° laminated DCB coupons. Very good consistency was found between the current solution Eq. (5(c)) and the FE results for all factors except E_{33} and G_{13}. The FE results were fully covered by Eq. (3(a)), Eq. (5(c)), and Eq. (6(c)).

3.3.1 A traction-separation law in a right-angled triangular form

Fig. 7 shows the profiles of l_{cz} and K versus σ_0 and G_c using the relationships expressed in

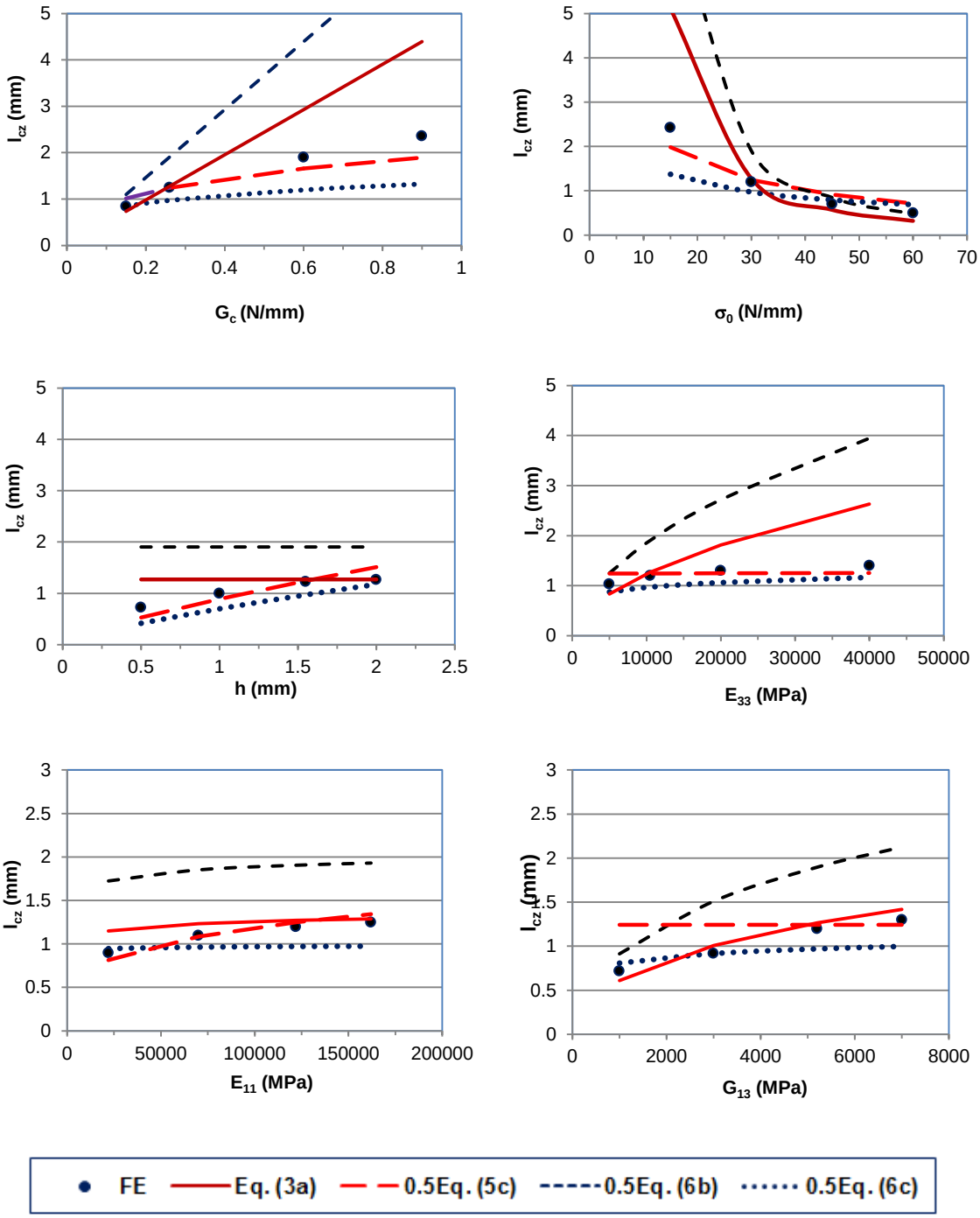

Fig. 5 Effect of specific parameters on the characteristic length profile of the HTA6376/C DCB coupon loaded in mode I

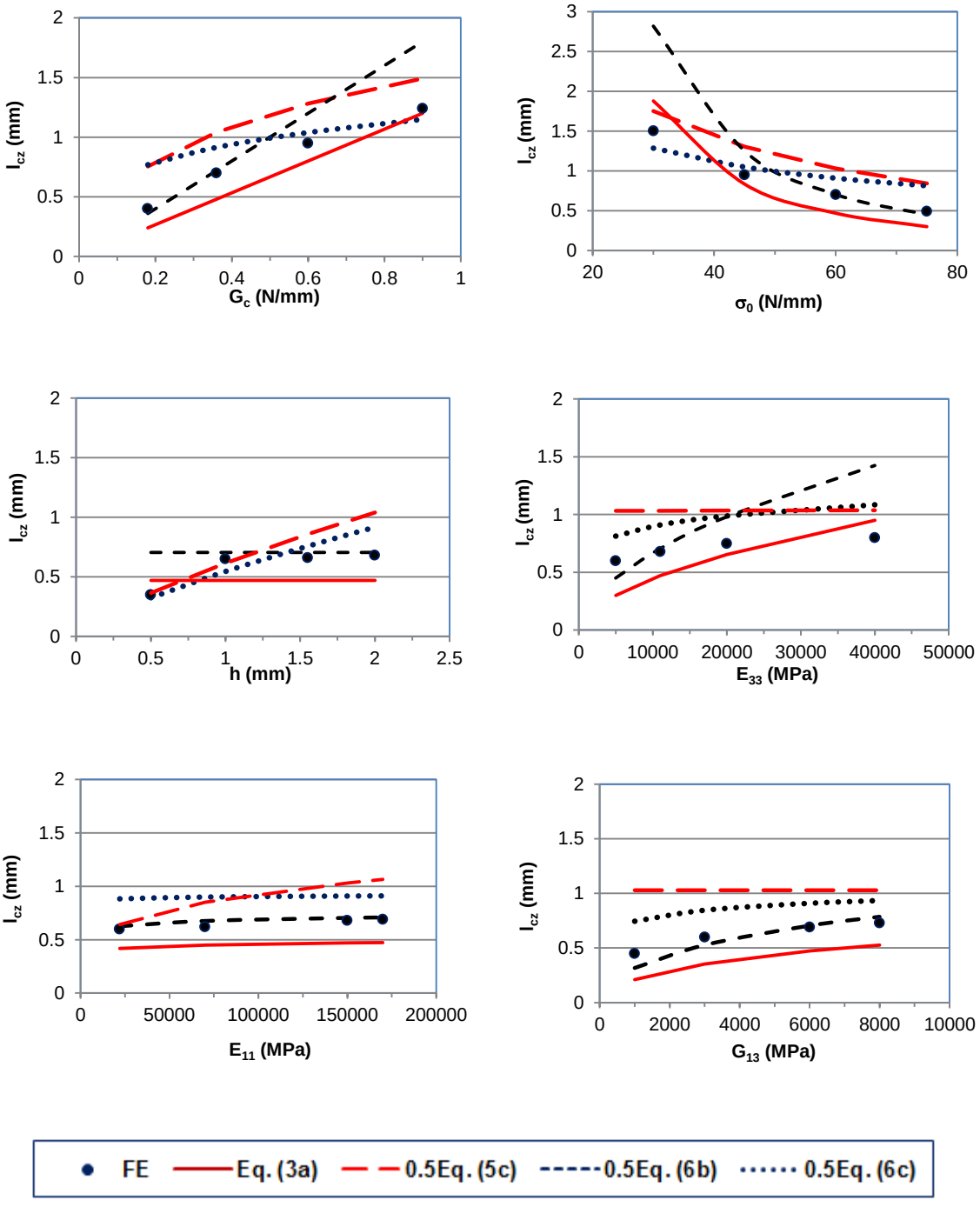

Fig. 6 Effect of specific parameters on the characteristic length profile of the T300/977-2 DCB coupon loaded in mode I

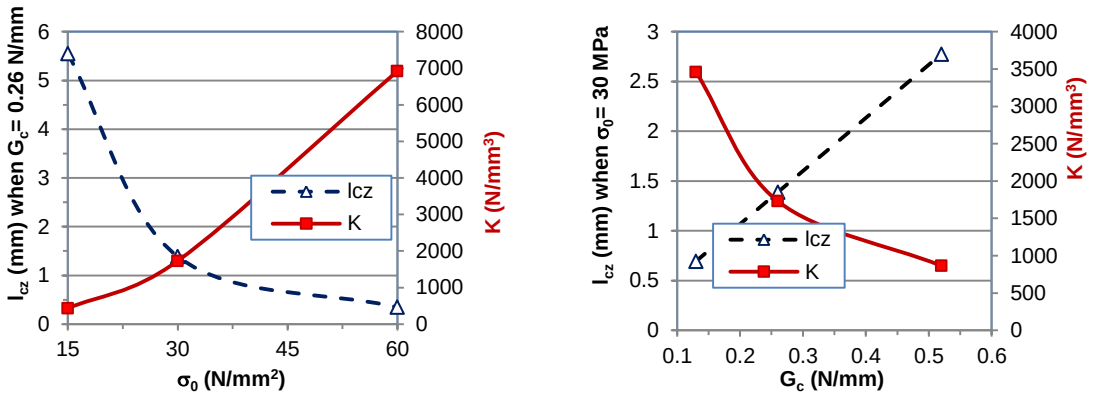

(a) (b)

Fig. 7 Profiles of l_{cz} and K versus σ_0 (a) and G_c (b) predicted by Eqs. (3(a)) and (7(d))

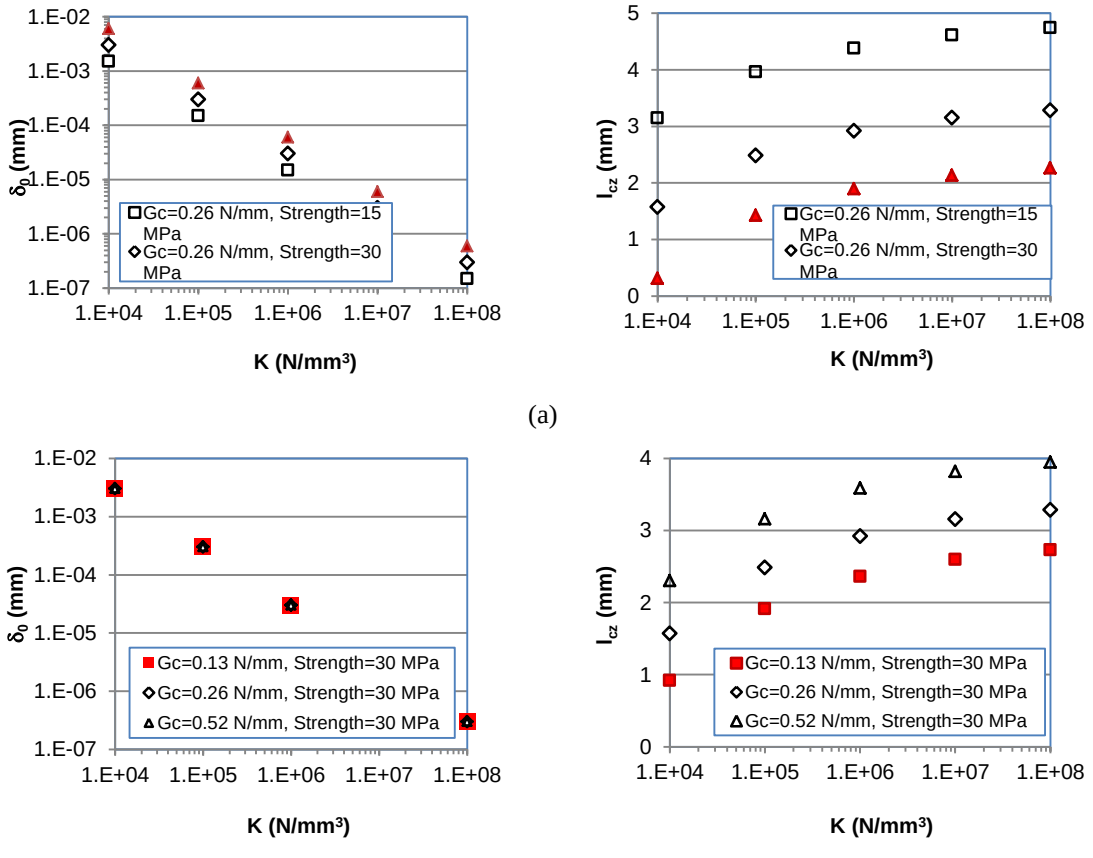

(a)

(b)

Fig. 8 Profiles of δ_0 and l_{cz} versus K and σ_0 (a), and K and G_c (b) predicted by Eq. (5(c)) for a bilinear traction-separation law

Eqs. (3(a)) and (7(d)). When the fracture energy, G_c, is kept constant, a large σ_0 will lead to a small l_{cz} and a large stiffness, K. When the interfacial strength, σ_0, is kept constant, a large G_c will extend l_{cz} and decrease the stiffness, K. Generally, the stiffness values are very small, and should be not used to an introduced cohesive zone for a practical progressive failure analysis. The results suggest that the interfacial strength, σ_0, should be large enough to ensure a high stiffness to prevent a significant effect on the transverse modulus of the original structures (Zou *et al.* 2002, Turon *et al.* 2007b). However, a large interfacial strength would lead to a small cohesive zone length. In addition, the right-angled triangular cohesive law has no progressive damage stage, resulting in a strong numerical singularity in its traction profile.

3.3.2 A bilinear cohesive traction-separation law

Profiles of δ_0 and l_{cz} versus σ_0 and K as well as G_c and K are shown in Fig. 8. It can be seen that a large interfacial strength will lead to a large separation displacement, δ_0. Physically, a large δ_0 will be at a location closer to the delamination tip than a small δ_0, which correlates with a small l_{cz}, as demonstrated in the figure. An increase in stiffness, K, would reduce the separation displacement, δ_0, creating a long l_{cz}. δ_0 is only related to the dependency rate of σ_0 over K, and has no direct relationship with G_c. However, when the interfacial strength is constant, a large G_c will lead to a large δ_0 at the delamination tip; thus, a fixed value of δ_0 will be relatively far from the delaminate tip and leads to a large l_{cz}. Individual factor of K, G_c, or σ_0 on the variation of l_{cz} can be studied analytically using the current solution of Eq. (5(c)), and Fig. 8 generated from the solution, Eq. (5(c)) based on the bilinear traction law, clearly demonstrates this logical judgment.

4. Conclusions

Theoretical explorations for determining the characteristic lengths of the cohesive zone for a double cantilever beam (DCB) specimen under mode I loading were conducted. The obtained two solutions expressed in Eqs. (3(a)) and (3(d)) for the right-angled triangular traction law, can be well fitted to the two existing solution groups presented in the open literature. They, Eqs. (3(a)) and (3(d)), are new additions to their associated groups expressed in Eqs. (6(a)) and (6(c)). For the bilinear cohesive traction-separation law, the graphical method can be feasibly used to determine the cohesive zone length based on the derived transcendental equation. As compared to existing analytical solutions, current solutions provided a better correlation with the FE results for most cases. Correlations among the cohesive law parameters were theoretically assessed for the two traction laws. For the right-angled triangular traction law, the three parameters are correlated to each other, and hence the individual effect on the cohesive zone length profile cannot be assessed. Furthermore, the stiffness usually is a small value. The bilinear traction law can effectively overcome these disadvantages. Any two parameters can be kept as invariables simultaneously when studying the effect of the third parameter on the variation of the cohesive zone length. In addition, the stiffness can be set to a high value, as required in the cohesive zone modeling approach, for a reasonable numerical progressive failure analysis. This work ensures that correlation of the cohesive element length with the cohesive zone length can be studied for the

identical bilinear traction law used in both theoretical and numerical methods; hence, a deep understanding of the FE results in the composite progressive failure analysis can be explored.

Acknowledgements

The work was carried out as part of a DND-DRDC funded project on Composite Structures. The financial support received from DND-DRDC and NRC Aerospace is greatly appreciated.

References

Alfano, G. (2006), "On the influence of the shape of the interface law on the application of cohesive-zone models", *Compos. Sci. Technol.*, **66**(6), 723-730.

Andersson, T.and Biel, A. (2006), "On the effective constitutive properties of a thin adhesive layer loading in peel", *Int. J. Fracture*, **141**(1-2), 227-246.

Bao, G. and Suo, Z. (1992), "Remarks on crack-bridging concepts", Appl. Mech. Rev., **45**(8), 355-366.

Chow, C.L., Woo, C.W. and Sykes, J.L. (1979), "On the determination and application of COD to epoxy-bonded aluminium joints", *J. Strain. Anal.*, **114**(2), 37-42.

Davis, M. and Bond, D. (1999), "Principles and practices of adhesive bonded structural joints and repairs", *Int. J. Adhesion. Adhes.*, **19(**2-3**)**, 91-105.

de Moura, M., Goncalves, J., Chousal, J. and Campilho, R. (2008), "Cohesive and continuum mixed-mode damage models applied to the simulation of the mechanical behavior of bonded joints", *Int. J. Adhesion. Adhes.*, **28**(8), 419-426.

Dias, G.F., de Moura, M.F.S.F., Chousal, J.A.G. and Xavier, J. (2013), "Cohesive laws of composite bonded joints under mode I loading", *Compos. Struct.*, **106**(12), 646-652.

Harper, P.W. and Hallett, S.R. (2008), "Cohesive zone length in numerical simulations of composite delamination", *Eng. Fract. Mech.*, **75**(16), 4774-4792.

Ji, G., Ouyang, Z., Li, G., Ibekwe, S. and Pang, S. (2010), "Effects of adhesive thickness on global and local Mode-I interfacial fracture of bonded joints", *Int. J. Solids Struct.*, **47**(18-19), 2445-2458.

Kanninen, M.F. (1973), "An augmented double cantilever beam model for studying crack propagation and arrest", *Int. J. Fracture*, **9**(1), 83-92.

Khoramishad, H., Crocombe, A.D., Katnam. K.B. and Ashcroft, I.A. (2010), "Predicting fatigue damage in adhesively bonded joints using a cohesive zone model", *Int. J. Fatigue*, **32**(7), 1146-1158.

Krenk, S. (1992), "Energy release rate of symmetric adhesive joints", *Eng. Fract Mech.*, **43**(4), 549-559.

Krueger, R. (2004), "The virtual crack closure technique: history, approach and application", *Appl. Mech. Rev.*, **57**(2), 109-143.

Landry, B. and Laplante, G. (2012), "Modeling delamination growth in composites under fatigue loading of varying amplitudes", *Compos. Part B*, **43**(2), 533-541.

Li, G., Johnston, A., Yanishevsky, M. and Bellinger, N.C. (2011), "Elastic deformation analysis of adhesively bonded composite butt joints in tension", *J. Aircraft*, **48**(2), 578-90.

Li, G., Chen, J.H., Yanishevsky, M. and Bellinger, N.C. (2012), "Static strength of a composite butt joint configuration with different attachments", *Compos. Struct.*, **94**(5), 1736-1744.

Li, G. and Li, C. (2013), "An analytical analysis of energy release rate in bonded composite joints in a mode I condition", *Compos. Part B*, **4**(1), 704-713.

Li, G. (2013), "Fatigue performance characterization of a composite butt joint configuration", *Compos. Part A*, **51**(8), 43-55.

Mi, Y., Crisfield, M.A. and Davies, G. (1998), "Progressive delamination using interface element", *J. Compos. Mater.*, **32**(14), 1246-1272.

Rybicki, E.F. and Kanninen, M.F. (1977), "A finite element calculation of stress intensity factors by a modified crack closure integral", *Eng. Fract. Mech.*, **9**(4), 931-939.

Turon, A., Costa, J., Camanho, P.P. and Davila, C.G. (2007a), "Simulation of delamination in composites under high-cycle fatigue", *Compos. Part A*, **38**(11), 2270-2282.

Turon, A., Davila, C.G., Camanho, P.P. and Costa, J. (2007b), "An engineering solution for mesh size effects in the simulation of delamination using cohesive zone models", *Eng. Fract. Mech.*, **74**(10), 1665-1682.

Williams, J.G. and Hadavinia, H. (2002), "Analytical solutions for cohesive zone models", *J. Mech. Phys. Solids*, **50**(4), 809-825.

Yang, Q. and Cox, B. (2005), "Cohesive models for damage evolution in laminated composites", *Int. J. Fracture*, **133**(2), 107-137.

Yang, Q., Cox, B., Nalla, R. and Ritchie, R. (2006), "Fracture length scales in human cortical bone: the necessity of nonlinear fracture models", *Biomaterials*, **27**(9), 2095-2113.

Zou, Z., Reid, S.R., Li, S. and Soden, P.D. (2003), "Modelling interlaminar and intralaminar damage in filament-wound pipes under quasi-static indentation", *J. Compos. Mater.*, **36**(4), 477-499.

Ashtonm, H.R. (1996), "Damage tolerance and durability testing for A/A-18 E/F composite materials structures", *Proceedings of the 37th AIAA/ASME/ASCE/AHS/ASC Structures, Structural Dynamics & Materials Conference*, Salt Lake City, UT, April, paper AIAA-96-1320-CP.

CC